Attitude Stability of a Dual-Spin Satellite with a Large Flexible Solar Array

D. B. CHERCHAS* AND P. C. HUGHES†
Institute for Aerospace Studies, University of Toronto, Toronto, Ontario, Canada

Attitude stability criteria and nutation decay times for a dual-spin satellite with a large flexible solar array are found. Both rotor and platform damping are included. A continuum mechanics analysis of the solar array develops practical information regarding array natural modes, and these represent additional degrees of freedom. With proper mass balancing, the equations for spin variables can be decoupled from those for transverse variables. Assuming the solar array to be rigid, the ratio of rotor inertia to the geometric mean of the vehicle transverse inertias must be greater than unity for stability unless there is energy dissipation in the despun section. This is a significant extension of the "major axis rule." Upper and lower stability boundaries exist for the nutation damper damping constant and the damper performance is best at high nutation frequencies. Introducing array flexibility leads to modifications of the stability boundaries when the nutation frequency becomes close to an array natural frequency.

Nomenclature

$\mathbf{a}_1, \mathbf{a}_2, \mathbf{a}_3$	= antenna reference axes
B	= bending stiffness of array supports
b_d	= damper wire length
c_d	= nutation damper coefficient
$I_{a_{ij}}$	= antenna inertia tensor (in F_A)
I_S	= rotor spin inertia
I_1, I_2	= satellite transverse inertias
m	= total satellite mass
m_d	= damper mass
m_s	= solar array mass
m_1	= $m_s(m - m_s)/(2m)$
m_2	= $1 - m_s/m$
m_3	= m_s/m
m_4	= $m - m_s$
N	= eigenvalue of nutational mode
P	= tension in array blanket
Q_j	= generalized (nonconservative) force
R	= inertia ratio $I_s/(I_1 I_2)^{1/2}$
$\mathbf{s}_1, \mathbf{s}_2, \mathbf{s}_3$	= solar array reference axes
T	= kinetic energy
U	= potential energy
y, z	= deflection in the Y, Z directions
x, y, z	= coordinates in array axes
x_{ac}, y_{ac}, z_{ac}	= antenna mass center relative to antenna reference point
x_{pc}, y_{pc}, z_{pc}	= array mount mass center relative to array mount reference point
$\mathbf{y}$	= state vector
α_1, α_2	= nutation/precession Euler angles
δ_1, δ_2	= angles defining orientation of pendulum damper
ω_n	= natural frequency of array (fixed base)
ω_N	= nutation frequency (rigid)
ω_S	= nominal rotor spin rate

Introduction

THE advantages of dual-spin for spacecraft attitude stabilization are now well known. However, as power requirements continue to escalate, it is clear that the body solar cells alone will not be able to generate the required power. This leads to designs which include, in addition to the previous dual-spin components, a large solar array (e.g., Fig. 1). Weight limitations imply significant structural flexibility and it is the present intention to discuss the implications of both the flexibility and the possible structural energy dissipation on dual-spin stability and performance.

The concept of "mono-spin" spacecraft stabilization is of fundamental importance in understanding "dual-spin" spacecraft attitude motion. Classically, a single rigid body in torque-free motion is stable in spin about its maximum or minimum axis of inertia. If the body contains a device which dissipates energy in response to nutational motion, then spin about the major axis is required for stability. Bracewell and Garriott[1] were the first to present expositions of this major axis rule. A dual-spin satellite is also capable of being spin stabilized. The gyroscopic stiffness is developed by revolving the two constituent bodies about their common spin axis in such a way that a significant amount of angular momentum exists along the spin axis. Perhaps, the most significant advance in dual-spin satellites was made in 1964–65 when it was noted independently by Landon[2] and Iorillo[3] that by insuring sufficient energy dissipation on the despun body, spin stabilization can be maintained at any ratio of rotor spin inertia to satellite transverse inertia despite rotor internal energy dissipation. These analyses assumed both bodies to be bodies of revolution about the common spin axis. The stability conditions were derived both from an energy-sink and from an infinitesimal approach and by stability analysis of the satellite equations of motion with an explicit damper model. A symposium[2] concerned with stability criteria of dual-spin satellites treated only configurations in which both spinning parts were bodies of revolution about the spin axis.

Likins[4] considered an asymmetric platform rigorously, but confined damping to the platform only; in the same paper[4] an energy sink argument was used heuristically to demonstrate

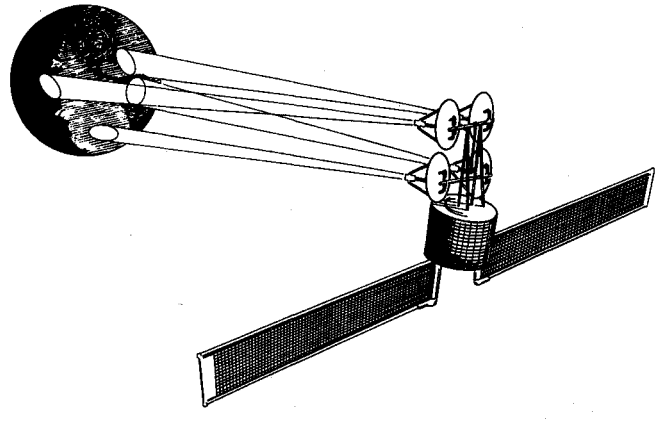

Fig. 1 Dual-spin communications satellite with large flexible solar array (Courtesy of Hughes Aircraft Co. Ltd).

Presented as Paper 72-887 at AIAA Guidance and Control Conference, August 14–16, 1972, Stanford, Calif.; received December 14, 1971; revision received September 13, 1972. Based on a doctoral dissertation by D. B. Cherchas.

Index category: Spacecraft Attitude Dynamics and Control.

* Formerly graduate student, presently Senior Structural Dynamicist, Spar Aerospace Products Ltd., Toronto.

† Associate Professor.

stability criteria for configurations which have damping in both bodies and an asymmetric platform.

The first rigorous treatment of a specific damping mechanism in both bodies (dashpots) was undertaken by Mingori[5] using the Floquet theory. Vigneron[6] studied a similar problem and demonstrated the method of averaging for problems of this type. In these papers[5,6] both bodies were assumed symmetrical. Analyses are rare in which the conditions a) asymmetric platform, b) damping in both bodies, and c) rigorous, are simultaneously met. Yet this is a case of practical importance.

The interest here is in the "despun-platform" case. This is a valid assumption for an Earth-pointing platform. If damping occurs only in the platform, the motion is always stable.[4] If damping occurs in both bodies, an energy-sink argument suggests that "energy losses in the spinning element are disadvantageous of stability of the rotor spin inertia is less than the average total transverse inertia."[4] In symbols, rotor damping is stabilizing if

$$I_S \geq (I_1 + I_2)/2 \quad \text{(energy sink)} \tag{1}$$

for energy loss in the rotor only. The "rigorous" analysis below for a particular configuration shows that it is the geometric mean, not the arithmetic mean, of the transverse inertias which is important; viz.

$$I_S \geq (I_1 I_2)^{1/2} \quad \text{(rigorous)} \tag{2}$$

For axisymmetric satellites, the two conditions, Eqs. (1) and (2), agree and in fact become the "major axis rule."

Criterion (2) may be supported by the physical argument of Landon.[2] He argued that the transverse angular velocity vector must rotate positively, relative to rotor-fixed axes, about the body axis along which spin is positive. Since the frequency of nutation (more correctly, the frequency of precession) is given by

$$\omega_N = I_S \omega_S / (I_1 I_2)^{1/2} \tag{3}$$

then the condition $\omega_N \geq \omega_S$ becomes precisely that given in Eq. (2).

A second purpose of this paper is to investigate the influence of flexibility on stability boundaries. For simple spinners, this issue has been largely resolved. The early work of Buckens[7,8] is relevant. A detailed review of this area will not be attempted here but contributions are noted by Vigneron,[9-11] Vigneron and Boresi,[12] Flatley,[13] Hughes,[14] Hughes and Fung,[15] and Meirovitch and Nelson.[16] Other references, as given in Meirovitch,[17] are also of interest.

In the sequel, the influence of flexibility on criterion (2) will be found, as well as on the criteria which correspond to Eq. (2) if there is damping in both bodies. Furthermore, the effects of pure flexibility are isolated from those of structural damping.

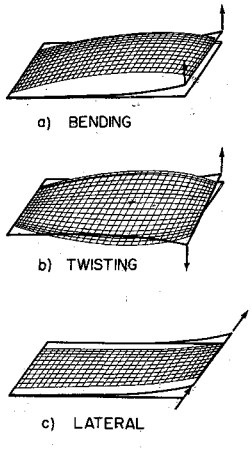

Fig. 2 Modal vibrations of solar array.

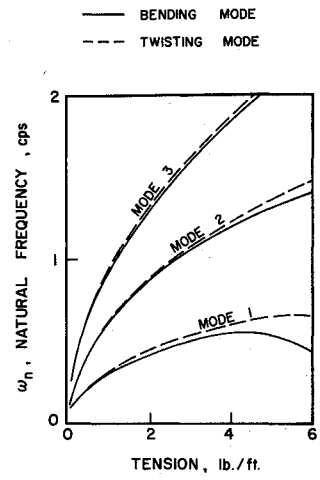

Fig. 3 Natural frequency vs sheet tension for bending and twisting modes.

Solar Array Flexibility

The natural vibration modes of the array (with a fixed base) are now determined. These modes will then be used to represent the degrees of freedom arising from array flexibility.

The array analyzed is based on the Hughes Aircraft FRUSA (Flexible Rolled-Up Solar Array).[18] The supporting booms (Fig. 1) are the well-known STEM or BISTEM booms (extendible booms manufactured by Spar Aerospace Products Ltd.) which can be rolled into a compact compartment until required. When the satellite is in its operational posture, booms and sheet are deployed into the final configuration shown in Fig. 1 with the sheet held in tension. A related array configuration is the T-boom type described by Coyner and Ross,[19] who employ finite-element considerations in their analysis.

Likins and Gale[20,21] approach the formulation of flexible dual-spin satellite equations by using a combination of discrete variables for the essentially rigid components and modal deformation coordinates for flexible appendages. This allocation of variables is termed the hybrid coordinate method.[22] The emphasis in these papers is on the influence of flexibility on the attitude and despin control systems. However, since no damping is included in the rotor, the effect of flexibility on the basic dual-spin criteria is not shown. Also, the use of small amounts of viscous damping in the appendage models may serve to mask some important effects. No dual-spin satellites with large flexible appendages have yet been flown.

The geometrical simplicity of the array suggests that the more traditional tools of continuum mechanics should be productive. A similar (T-boom) array has been dealt with in this fashion by Hughes.[23,24] A partial differential equation of motion is written for each principal array element (Fig. 2)—namely, each of the two booms, the sheet, and the tip piece.[25] Appropriate boundary conditions must also be included. Each boom is approximated as a thin cantilevered beam. The sheet is modeled as a membrane (no bending stiffness) in a state of uniform longitudinal tension; however, the structure is assumed to be such that no wrinkling can occur at least for small lateral in-plane deflections. The tip piece is assumed rigid. For brevity, and to avoid introducing a plethora of new symbols, the reader is referred to Cherchas[25] for details. The final result is that a certain determinant must be zero, whose elements are transcendental functions of the frequency of vibration. This condition specifies a countably infinite set of natural frequencies.

As suggested by Fig. 2, these natural modes may be subdivided into three classes, referred to below as "bending," "twisting,"

Table 1 Array parameters

Length = 18.2 ft; width = 6 ft
Support boom mass density = 0.195 lb-ft^{-1}
Support boom bending stiffness = 3.32 × 10^5 lb-in.^{2}
Blanket mass density = 0.25 lb-ft^{-2}
Blanket Young's modulus = 7 × 10^6 psi

and "lateral." In the bending mode, both booms and the sheet vibrate in the same direction, out of the nominal plane; the boom deflections are equal and the sheet's deflection is not a function of distance across its width. The twisting mode is a rotation about the array centerline. The boom and sheet deflections are symmetrical with respect to the centerline. In the lateral mode, the array deflects only in the nominal plane and both booms have the same deflection.

Figure 3 indicates some typical results. From a design standpoint, the dependence of natural frequency on sheet tension is important. The parameters listed in Table 1 were selected and are representative. Figure 3 shows the first three natural frequencies vs tension (bending and twisting modes). For tensions which are much less than the critical value (which buckles the supporting booms) the behavior is essentially that of a sheet in tension, and fixed at both ends. With greater tension, the boom begins to play a role and a decrease in frequency appears. The first natural frequencies diminish to zero at the Euler critical load for a boom with pinned/pinned end constraints. For lateral vibrations, the frequencies are considerably higher.[25]

Spacecraft Attitude Motion

The equations governing the motion of the satellite about its mass center are written from Lagrange's equations

$$d/dt\left(\frac{\partial T}{\partial \dot{q}_j}\right) - \partial T/\partial q_j + \partial U/\partial q_j = Q_j \tag{4}$$

The generalized coordinates q_j chosen are described below.

Figure 4 shows the reference axes used to formulate the mathematical rotation angles simulation. The coordinates relate the axis sets with 3, 2, 1 Euler angles as follows:

$$F_I \to F_A, \alpha_3, \alpha_2, \alpha_1; \quad F_R \to F_F, \phi_3, \phi_2, \phi_1$$
$$F_A \to F_D\ 0, \delta_2, \delta_1; \quad F_R \to F_P, \gamma_3, 0, 0$$
$$F_A \to F_P\ \psi_3, 0\ 0; \quad F_P \to F_S, 0, 0, \lambda_1$$

The vector $\mathbf{d}$ is described relative to F_S by array natural mode deformations. The deflections of the array relative to the F_S set are described by expansions of the form

$$v(x, z, t) = \sum \varepsilon_i(t) S_i(x) + \sum \mu_i(t) T_i(x, z)\Big|_{a \text{ or } b} \tag{5}$$

$$w(x, t) = \sum v_i(t) L_i(x)\Big|_{a \text{ or } b} \tag{6}$$

where S_i, T_i, L_i are the bending, twisting, and lateral mode shapes, respectively. The subscript a refers to the array on the positive d_1 side and b to that on the negative d_1 side. ε_{ai} and ε_{bi} represent symmetric mode deflections along the $\mathbf{s}_1$ axis and v_{ai}, v_{bi} are deflections in the $\mathbf{s}_3$ direction for the lateral mode. The generalized coordinate ψ_3 is redescribed by $\psi_3 = \omega_S t + \beta$ where ω_S is the nominal rotor spin rate relative to inertial axes.

The total kinetic energy for the satellite can be expressed as

$$T = \tfrac{1}{2}\sum \boldsymbol{\omega}_j{}^T I_j \boldsymbol{\omega}_j + \tfrac{1}{2}\sum m_j \dot{\boldsymbol{\rho}}_j \cdot \dot{\boldsymbol{\rho}}_j - (1/2m)(\sum m_j \dot{\boldsymbol{\rho}}_j)\cdot(\sum m_j \dot{\boldsymbol{\rho}}_j)$$
$$+ m_1[(\boldsymbol{\omega}_a \cdot \boldsymbol{\omega}_a)(\mathbf{P}\cdot\mathbf{P}) - (\boldsymbol{\omega}_a \cdot \mathbf{P})^2] - m_3 \boldsymbol{\Omega}\cdot\sum m_j \dot{\boldsymbol{\rho}}_j$$
$$+ m_2 \boldsymbol{\Omega}\cdot\int \dot{\mathbf{d}}\, dm - (1/m)(\sum m_j \dot{\boldsymbol{\rho}}_j)\cdot\int \dot{\mathbf{d}}\, dm + \tfrac{1}{2}\int \dot{\mathbf{d}}\cdot\dot{\mathbf{d}}\, dm$$
$$- (1/2m)(\int \dot{\mathbf{d}}\, dm)\cdot(\int \dot{\mathbf{d}}\, dm)$$

where $\int$ is over appendage mass, $\sum_j$ is over-all satellite parts except the appendages. $\mathbf{P} = \mathbf{r}_p - \mathbf{d}_a$, $\boldsymbol{\Omega} = \boldsymbol{\omega} \times \mathbf{P}$, $\boldsymbol{\omega}_a$ = angular velocity of antenna, and $\boldsymbol{\omega}_j$, $\dot{\boldsymbol{\rho}}_j$ are the rigid component angular velocities and centroidal velocities relative to the combined mass center.

The internally stored potential energy is due to the elastic strain energy in the booms and in the deformed tensioned sheets; i.e.,

$$U \simeq \sum_n \frac{B}{2}\int (v_{xx}{}^2 + w_{xx}{}^2)\, dx + \sum_m \frac{P}{2}\iint (v_x{}^2 + w_x{}^2)\, dx\, dz + k_d(\delta_1{}^2 + \delta_2{}^2) \tag{8}$$

where n = number of booms, m = number of sheets.

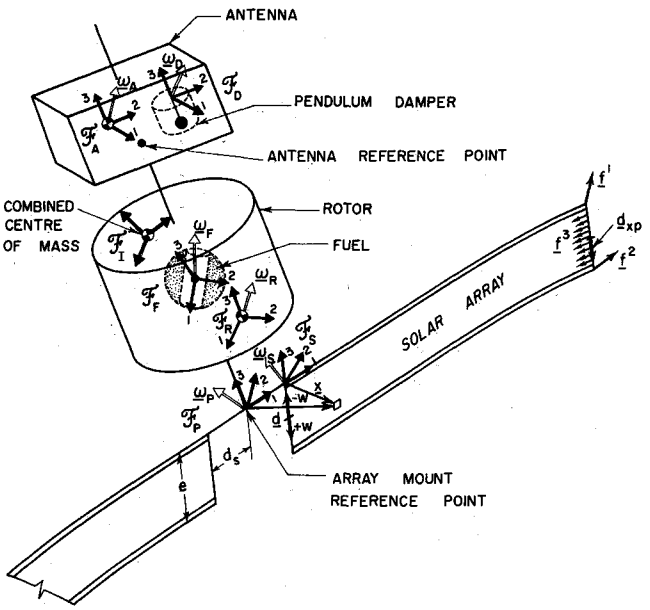

Fig. 4 Satellite coordinate axes.

The generalized forces originate from the resistance to damper ball motion offered by the damper fluid and the viscous resistance generated in the boundary layer of the liquid propellant. The damper generalized forces are

$$Q_{\delta_1} = -c_d b_d{}^2\, \dot{\delta}_1, Q_{\delta_2} = -c_d b_d{}^2\, \dot{\delta}_2 \tag{6}$$

The viscous resistance generated in the boundary layer by the fuel in contact with tank wall causes a torque $\boldsymbol{\tau}_f$ to appear as the fuel bulk moves in its cavity. $\boldsymbol{\tau}_f$ can be found by integrating, over the entire boundary layer, the force times the appropriate moment arm about the fuel mass center. This modeling is similar to that used by Barba.[2] In fuel axes, to first order,

$$\boldsymbol{\tau}_f \simeq \begin{bmatrix} I_{s_1} c_f & 0 & 0 \\ 0 & I_{s_1} c_f & 0 \\ 0 & 0 & I_{s_3} c_f \end{bmatrix} \begin{bmatrix} \dot{\phi}_1 \\ \dot{\phi}_2 \\ \dot{\phi}_3 \end{bmatrix}$$

where $c_f = (\Omega_n \rho_f \mu/2)^{1/2}$, ρ_f = mass density of fuel, μ = viscosity of fuel, and Ω_n = frequency of fuel oscillation relative to cavity. Furthermore, the moments of area about each axis are

$$I_{s_1} = \tfrac{2}{3}\pi R_f{}^4(4 - c^2)(1 - c^2)^{1/2}$$
$$I_{s_3} = \tfrac{4}{3}\pi R_f{}^4(2 + c^2)(1 - c^2)^{1/2}$$

where $c = r_f/R_f$, R_f = radius of spherical cavity, and r_f = radius of cylindrical hollow. Therefore the corresponding generalized forces are, to first order,

$$Q_{\phi_1} = -\tau_{f_1}, Q_{\phi_2} = -\tau_{f_2}, Q_{\phi_3} = -\tau_{f_3} \tag{10}$$

for $q_j = \phi_1$, ϕ_2, and ϕ_3, respectively.

Linear Equations

Lagrange's equations of motion for the satellite are derived by inserting T, U, and Q_j into Eq. (7). The resulting equations are then linearized by neglecting quantities second-order or higher in the generalized coordinates α_1, α_2, α_3, δ_1, δ_2, β, ϕ_1, ϕ_2, ϕ_3, $\ddot{\gamma}_3$, ε_i, μ_i, v_i. It is further assumed that the rotor is perfectly balanced, that the nominal spin rates of the antenna and array are approximately zero, and that the antenna is symmetric about the $\mathbf{a}_1 - \mathbf{a}_3$ plane. Also, the transformation

$$\begin{bmatrix} \phi_1 \\ \phi_2 \\ \phi_3 \end{bmatrix} = \begin{bmatrix} c\psi_3 & s\psi_3 & 0 \\ -s\psi_3 & c\psi_3 & 0 \\ 0 & 0 & 1 \end{bmatrix} \begin{bmatrix} \xi_1 \\ \xi_2 \\ \xi_3 \end{bmatrix} \tag{11}$$

is made to remove the periodic coefficients from the equations. The generalized forces corresponding to those in Eq. (10) are

$$Q_{\xi_1} = -I_{s_1} c_f(\dot{\xi}_1 + \omega_S \xi_2); \quad Q_{\xi_2} = -I_{s_1} c_f(\dot{\xi}_2 - \omega_S \xi_1);$$
$$Q_{\xi_3} = -I_{s_1} c_f \dot{\xi}_3 \tag{12}$$

The rather lengthy equations of motion may now be written[25] from Eq. (4) using these simplifications and the T, U, and Q_j given by Eqs. (7–9 and 11).

It is clear that it would be advantageous to decouple the equations involving the nutation variables from those involving the spin variables since this would make the despin control problem easier. This desirable decoupling can be accomplished (in the linearized equations) by requiring x_{ac}, I_{a13}, I_{a23}, y_{pc}, x_{pc}, and λ_1 to be zero. λ_1 is usually zero on proposed satellites of the type under study here and the first five quantities can be set to zero by balancing the antenna and array mount. This decoupling also implies certain restrictions on mode shapes which are met here but not generally. Since the essence of the study is to determine basic stability criteria, it is assumed that the mass balancing required for decoupling has been done, and that the despin control systems are working perfectly in keeping the nominal antenna and array spin rates desired (here approximated as zero). The resulting simplified equations serve as an excellent basis for study and may be expected to reveal the intrinsic dual-spin criteria.

Stability and Performance

The decoupled nutation variable equations are now written in first-order form, $\dot{\mathbf{y}} = \mathbf{M}\mathbf{y}$, say,‡ and stability criteria evolved numerically from the requirement that the eigenvalues of $\mathbf{M}$ have negative real parts.

To decrease by one the number of independent parameters that need be varied, the damper stiffness is adjusted so that the undamped natural frequency of the damper, $(k_d/m_d b_d^2)^{1/2}$, is equal to the despun platform nutation frequency which, if the satellite were rigid, would be given by Eq. (3). This "tuning" has been shown by Cloutier[27] to be optimum for dissipating nutational energy in a rigid satellite system. A characteristic nutation decay time (the measure of "performance" used herein) can be found by examining the real parts of the eigenvalues of satellite nutational modes. The sensitivities of performance to significant satellite parameters are important design characteristics.

There are some physical factors about the satellite that require interpretation in order to conduct an eigenvalue study. The variables α_1, α_2 do not appear because the environmental torques which would be a function of attitude (i.e., α_1, α_2) are not included and linearization removes any remaining terms involving α_1 and α_2 from the torque-free equations. The order of the system can thus be reduced by considering $\dot{\alpha}_1$, $\dot{\alpha}_2$ as the nutation variables and removing α_1 and α_2 from the state vector. Next, considering array vibrations, if no array damping is used then there will be some satellite natural modes that have zero real parts. An example of such an eigenvector would be counter-rotating twisting modes of the array. This vibration can exist independently of any other motion. Due to numerical error, the computed real parts may be slightly nonzero—i.e., a pure oscillation would appear numerically to have a slowly decaying or growing amplitude. It is desirable to avoid the confusion caused by these numerically generated instabilities; that is, the numerical search for instability is conducted so that undamped "purely appendage" modes are not taken as unstable. This is done by replacing the condition $Re(N) > 0$ by $Re(N) > \varepsilon > 0$, where ε is some small positive number. In practical terms there is essentially no difference between these two requirements; the device is employed only for numerical convenience. The eigenvectors whose stability is of interest involve the nutation variables α_1, α_2. In fact, these eigenvectors are identified as those which suggest predominantly α_1 and α_2 motion. The numerical determination of stability criteria and performance (i.e., nutation damping times) is undertaken from four points of view, each giving further useful insight into the dual-spin dynamics.

‡ Here $\mathbf{y}$ is the state vector, $\mathbf{y}I = (\dot{\alpha}_1, \dot{\alpha}_2, \dot{\delta}_1, \dot{\delta}_2, \dot{\varepsilon}_{ai}, \dot{\varepsilon}_{bi}, \dot{\mu}_{ai}, \dot{\mu}_{bi}, \dot{\nu}_{ai}, \dot{\nu}_{bi}, \alpha_1, \alpha_2, \delta_1, \delta_2, \varepsilon_{ai}, \varepsilon_{bi}, \mu_{ai}, \mu_{bi}, \nu_{ai}, \nu_{bi})$.

c_d Stability Range

Given that the nutation damper is tuned as described earlier, the range of the damping coefficient in which satellite nutational motion is stable is of prime interest. This range is established in terms of satellite inertia ratio R and rotor spin rate ω_S. Figure 5 shows the stability boundaries determined from $Re(N) > 0$ with the array assumed rigid. The stability criteria can be determined from $Re(N) > \varepsilon = 0$ because no flexible array modes appear. The inertia ratio is varied by changing the rotor radius and keeping all other parameters fixed except, of course, c_d. In varying the rotor radius, it is assumed that the rotor is mass homogeneous. Based on rotor mass and initial inertias, the initial radius and height for an equivalent homogeneous cylinder are calculated and then, by varying the radius, the rotor inertia ratio is adjusted. The parameters used are given by Cherchas.[25] These values describe a typical dual-spin configuration (based on TACSAT I data) with a compatible array attached. The behavior indicated on Fig. 5 shows that both too little and too much damping will result in instability for inertia ratios less than 1. The upper boundary, illustrated for a typical rotor spin rate, represents the fact that if the damper viscous resistance becomes too great, the response to nutational motion will not yield sufficient energy dissipation to counteract the rotor damping which tends to destabilize. As the inertia ratio approaches 1,

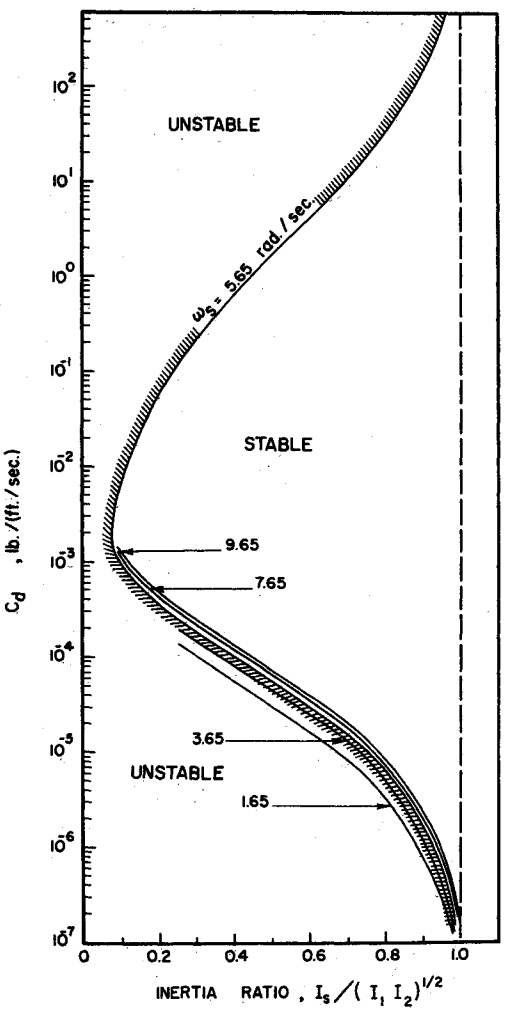

Fig. 5 Stability boundaries, rigid array, $Re(N) > 0$.

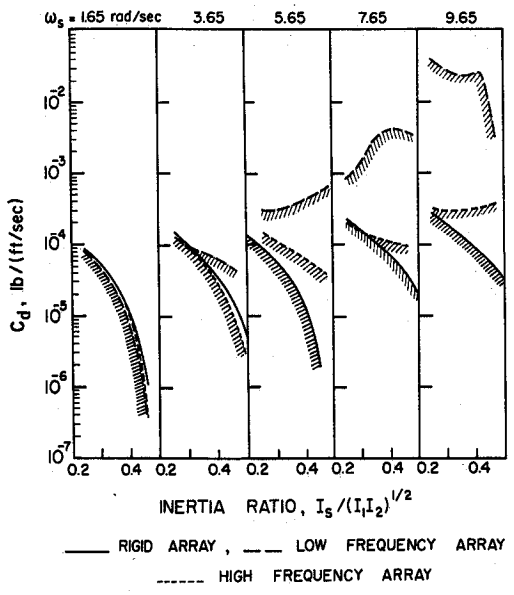

Fig. 6 C_d Stability boundaries, $Re(N) > 10^{-4}$. [High frequency array natural frequencies (cps): bending—1.026, 2.127, 3.255; twisting—1.084, 2.189, 3.301; lateral—8.375. Low frequency array natural frequencies (cps): bending—0.513, 1.064, 1.627; twisting—0.542, 1.095, 1.651; lateral—4.52].

the stable range of c_d becomes greater. This can be explained by recognizing that at an inertia ratio of 1, the nutation frequency as seen in rotor fixed axes is zero; thus, the fuel will contribute no damping.[25]

A significant point illustrated by Fig. 5 is that, for a given damper mass, it is possible that an optimum damper will not be able to achieve satellite stability below a certain inertia ratio. This fact has not been pointed out in the literature except by implication in equations similar to Eq. 6 of Ref. 3. The lower inertia ratio boundary is rather significant, as the trend in dual-spin satellites is to lower inertia ratios.

Figure 6 shows the stability boundaries of Fig. 5, determined now from $Re(N) > 10^{-4}$, for a portion of the inertia ratio range. The stability boundaries for the same configuration but including array flexibility for a low- and high-frequency solar array are shown as well. The frequencies of the low- and high-frequency arrays are indicated in Fig. 6. The total array mass is not changed between the two array cases, but the boom diameter has been increased to accommodate the higher tension in the sheet for the high-frequency case. The boom mass density is unchanged.

When the spin rate and inertia ratio are low enough so that the nutation frequency of the despun components is well below the lowest natural frequency of the array, the effect of flexibility is very small. However, when the nutation and array frequency are about equal, the undamped flexibility significantly affects the stability properties. The greatest effect occurs when the frequency of the nutation equals an array natural frequency. This is evidenced by noting that at the inflection point of the low frequency array boundaries for $\omega_S = 7.65, 9.65$ rad/sec in Fig. 6, the frequency of the satellite's main nutation mode is approximately 0.5 cps. The stability boundaries which include array flexibility are found using one mode for each of the degrees of freedom of the array. No significant change in the stability boundaries is observed by increasing the number of array modes used.

Performance—Decay Time of Nutation Modes

The damping time of the nutation modes gives a direct indication of the damper performance. This performance is determined below as a function of satellite inertia ratio and rotor spin rate. Figure 7 is a plot of $-Re(N)$ for the main nutation mode assuming a rigid array. The basic parameters are the same as

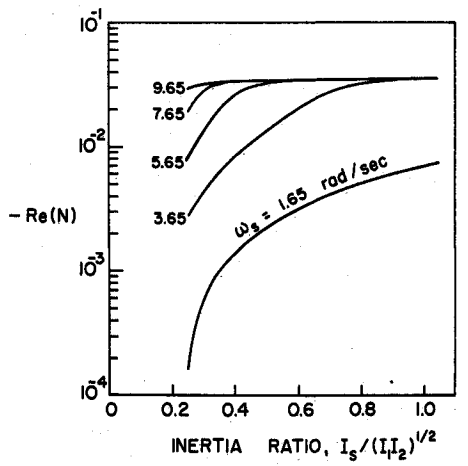

Fig. 7 Performance of nutation modes, rigid array, balanced antenna and array mount.

in the foregoing stability studies with $c_d = 0.015$ lb-sec-ft^{-1}. It is clear that the damper performs better at high spin rates and inertia ratios, that is, at high nutation frequencies.

These calculations are repeated with flexibility, but no array damping for the low-frequency array. Figure 8 depicts the results using two modes in both the twisting and bending degrees of freedom. In Fig. 9, 0.2% critical damping is assumed for each array mode (linear viscous damping). The linear viscous model is not an accurate statement of array damping mechanisms;[27] however, it is used here to show the effect of an array damping model on the stability results. The results in Figs. 7–9 show that flexibility has little effect on the damping time of the satellite nutation modes except when the nutation mode frequencies become close to the array natural frequencies; this effect is the greatest when the nutation and array frequencies are the same. To recognize this behavior, note in Fig. 8 that the lowest array frequency ($\sim$0.5 cps) falls in the range of nutation frequency of the drastic drops in $-Re(N)$. The slight drops on the high-inertia ratio end of $\omega_S = 7.65, 9.65$ rad/sec curves are similar resonances for the second array natural frequency ($\sim$1 cps). Figure 9 clearly shows that array damping can have a large effect and can easily mask the effects of flexibility alone. That is, by comparing Figs. 8 and 9, it is evident that only the somewhat unpredictable array damping is keeping the satellite stable in some regions. In this respect, it should be noted that when the nutation frequency is close to an array natural frequency, the appendage acts as an excellent nutation damper.

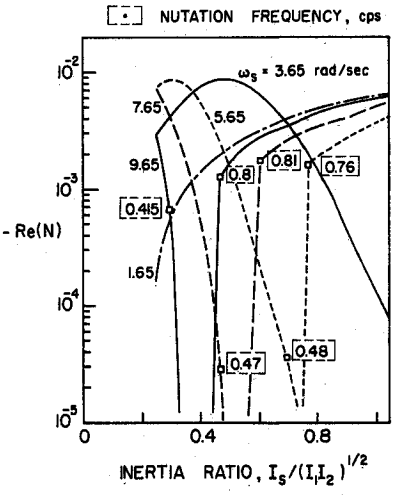

Fig. 8 Performance of nutation modes, flexible (2,2,1), low frequency array, balanced antenna and array mount, 0% critical damping in array. [Array frequencies (cps): bending—0.513, 1.064; twisting—0.542, 1.095; lateral—4.52].

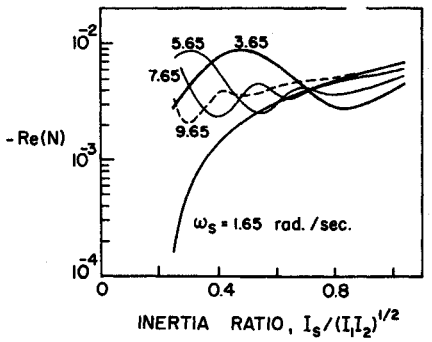

Fig. 9 Performance of nutation modes, flexible (2,2,1) low frequency array, balanced antenna and array mount, 0.2% critical damping in array. [Array frequencies (cps): bending—0.513, 1.064; twisting—0.542, 1.095; lateral—4.52].

Major Axis Rule Generalized

Another basic configuration is now chosen to further investigate the dependence of satellite stability on the inertia ratio $I_S/(I_1I_2)^{1/2} = R$. The despun portion has significantly different transverse inertias while the rotor is symmetric. By reducing the damping efficiency of the damper to zero and varying the rotor inertia ratio, stability boundaries are established for the rigid and undamped/flexible configurations. The array is mounted on the same end of the rotor as the antenna. The results indicate how the rule [Eq. (2)] is modified by flexibility. Using a realistic set of parameters,[25] the inertia ratio is varied by changing the rotor radius only. Figure 10 shows the stability boundary assuming a rigid array based on $Re(N) > 0$, $> 10^{-6}$, and the same boundary with the flexibility of the high frequency array included but without array damping. It is observed that $R = 1$ represents, for the rigid systems, the stability boundary (damping only in the rotor). This rule is altered with flexibility and, in fact, the ratio must be $> R^*$ for stability, where $R^*(\omega_S)$ is the new boundary ($R^* \geqslant 1$).

Conclusions

The foregoing investigation has produced some significant conclusions. With regard to the solar array, the lowest frequency modes are likely going to be primarily sheet modes, and the frequency of this mode can only be raised to a certain point by increasing tension.

The importance of the inertia ratio $R = I_S/(I_1I_2)^{1/2}$ has been demonstrated with unity as the pivotal value (despun platform). For the rigid satellite considered, and damping in the rotor, stability is always possible if $R > 1$. Note that this condition is less strict than in Eq. (1) for asymmetric bodies. If $R < 1$, the nutation damper constant must lie in a range $c_{d_1}(R) \leqslant c_d \leqslant c_{d_2}(R)$ as indicated by Fig. 5. For a given damper mass, it is not always possible to stabilize if R is too small. It has also been shown that the tuned damper is most effective in reducing nutation at high nutation frequencies.

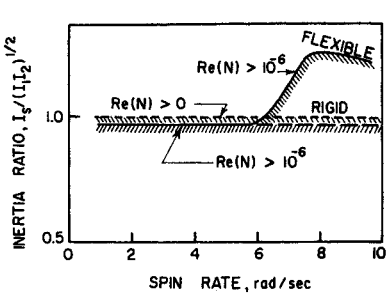

Fig. 10 Inertia ratio stability boundary, rigid array $Re(N) > 10^{-6}$ and flexible (1,1,1) high frequency array, $Re(N) > 10^{-6}$. [Array frequencies (cps): bending—1.026; twisting—1.084; lateral—8.375].

When the flexibility of the appendage is included, the stability criteria and nutation damping times are altered little from rigid results if the appendages have natural frequencies well above the nutation frequency. However, when ω_N is within $\sim 25\%$ of ω_n, the stability criteria are significantly and undesirably affected. It has been shown also that the use of a small amount of viscous damping in the appendage will mask the effects of flexibility. The designer must ensure that the presumed stability is not due entirely to the somewhat unpredictable damping in the solar array.

References

[1] Bracewell, R. N. and Garriott, O., "Rotation of Artificial Earth Satellites," *Nature*, Vol. 182, Sept. 1958, pp. 760–762.

[2] *Proceedings of the Symposium on Attitude Stabilization and Control of Dual-Spin Spacecraft*, Air Force Rept. SAMSO-TR-68-191, Air Force Systems Command; also Aerospace Corp. Rept. TR-0158 (3307-01)-16, Nov. 1967, El Segundo, Calif.

[3] Iorillo, A. J., "Nutation Damping Dynamics of Rotor Stabilized Satellites," presented at the ASME Annual Winter Meeting, Chicago, Ill., Nov. 1965.

[4] Likins, P. W., "Attitude Stability Criteria for a Dual-Spin Spacecraft," *Journal of Spacecraft and Rockets*, Vol. 4, No. 4, April 1967, pp. 1638–1643.

[5] Mingori, D. L., "The Effects of Energy Dissipation on the Attitude Stability of Dual-Spin Satellites," *AIAA Journal*, Vol. 7, No. 1, Jan. 1969, pp. 20–26.

[6] Vigneron, F. R., "Stability of a Dual-Spin Satellite with Two Dampers," *Journal of Spacecraft and Rockets*, Vol. 8, No. 4, April 1971, pp. 386–389.

[7] Buckens, F., "The Influence of Elastic Components on the Attitude Stability of a Satellite," *Proceedings of the 5th International Symposium on Space Technology and Science*, Tokyo, Japan, 1963.

[8] Buckens, F., "On the Influence of the Elasticity of Components in a Spinning Satellite on the Stability of Its Motion," *Proceedings of the 16th IAF Congress*. Athens, Greece, 1965.

[9] Vigneron, F. R., "Dynamics of Spin-Stabilized Flexible Satellites of Crossed-Dipole Configuration," *Dynamics of Satellites*, Springer-Verlag, New York, 1970.

[10] Vigneron, F. R., "Stability of a Freely Spinning Satellite of Cross-Dipole Configuration," *CASI Transactions*, Vol. 3, No. 1, March 1970 pp. 8–19.

[11] Vigneron, F. R., "Effects of Earth's Gravitational Forces in the Flexible Crossed-Dipole Satellite Configuration—Part 2, Attitude Stability," *CASI Transactions*, Vol. 3, No. 2, Sept. 1970, pp. 127–134.

[12] Vigneron, F. R. and Boresi, A. P., "Effect of Earth's Gravitational Forces on the Flexible Crossed-Dipole Satellite Configuration—Part 1, Configuration Stability and Despin," *CASI Transactions*, Vol. 3, No. 2, Sept. 1970, pp. 115–126.

[13] Flatley, T. W., "Attitude Stability of a Class of Partially Flexible Spinning Satellites," TN D-5268, Aug. 1969, NASA.

[14] Hughes, P. C., "Satellite Stability," *CASI Transactions*, Vol. 3, No. 2, Sept. 1970, p. 170.

[15] Hughes, P. C. and Fung, J. C., "Liapunov Stability of Spinning Satellites With Long Flexible Appendages," *Celestial Mechanics Journal*, 4, 1971, pp. 295–308.

[16] Meirovitch, L. and Nelson, H. D., "On the High-Spin Motion of a Satellite Containing Elastic Parts," *Journal of Spacecraft and Rockets*, Vol. 3, No. 11, Nov. 1966, pp. 1597–1602.

[17] Meirovitch, L., "Stability of a Spinning Body Containing Elastic Parts via Liapunov's Direct Method," *AIAA Journal*, Vol. 8, No. 7, July 1970, pp. 1193–1200.

[18] Wolff, G., "Oriented Flexible Rolled-Up Solar Array," AIAA Paper 70-738, Los Angeles, Calif., 1970.

[19] Coyner, J. V. and Ross, R. G., "Analysis of Performance Characteristics and Weight Variations of Large Area Roll Up Solar Arrays," presented at the ASME Annual Winter Meeting, Los Angeles, Calif., Nov. 1969.

[20] Likins, P. W. and Gale, A. H., "The Analysis of Interactions Between Control Systems and Flexible Appendages," Paper AD-29, presented at the 19th Congress of the International Astronautical Federation, New York, Oct. 1968.

[21] Gale, A. H. and Likins, P. W., "Influence of Flexible Appendages on Dual-Spin Spacecraft Dynamics and Control," *Journal of Spacecraft and Rockets*, Vol. 7, No. 9, Sept. 1970, pp. 1049–1056.

[22] Likins, P. W. and Wirsching, P. H., "Use of Synthetic Modes in

Hybrid Coordinate Dynamic Analysis," *AIAA Journal*, Vol. 6, No. 10, Oct. 1968, pp. 1867–1872.

[23] Hughes, P. C., "Flexibility Considerations for the Pitch Attitude Control of the Communications Technology Satellite," *CASI Transactions*, Vol. 5, No. 1, March 1972, pp. 1–4.

[24] Hughes, P. C., "Attitude Dynamics of a Three-Axis Stabilized Satellite With a Large Flexible Solar Array," *Journal of Astronautical Sciences*, to be published.

[25] Cherchas, D. B., "Attitude Stability and Performance of a Dual-Spin Satellite With Large Flexible Appendages," Rept. 170, Oct. 1971, Univ. of Toronto Institute for Aerospace Studies, Toronto, Ontario, Canada.

[26] Lamb, H., *Hydrodynamics*, 6th ed., Dover, New York, p. 622.

[27] Cloutier, G. J., "Nutation Damper Design Principles for Dual-Spin Spacecraft," *Journal of the Astronautical Sciences*, Vol. 16, No. 2, March–April 1969, pp. 79–87.

[28] Graham, W. B., "Linear Dynamics of Damped Cantilever Beams With Applications to a Symmetric Twin-Boom Satellite," M.A.Sc. thesis, 1971, Univ. of Toronto Institute for Aerospace Studies, Toronto, Ontario, Canada.

FEBRUARY 1973 J. SPACECRAFT VOL. 10, NO. 2

Orbit Determination by Range-Only Data

NGUYEN DUONG* AND C. BYRON WINN†
Colorado State University, Fort Collins, Colo.

The determination of satellite orbits for use in geodesy using range-only data has been examined. A recently developed recursive algorithm for rectification of the nominal orbit after processing each observation has been tested. It is shown that when a synchronous satellite is tracked simultaneously with a subsynchronous geodetic target satellite, the orbits of each may be readily determined by processing the range information. Random data errors and satellite perturbations are included in the examples presented.

Nomenclature

a	= semimajor axis of satellite orbit, Earth radii
e	= eccentricity of satellite orbit, nondimensional
i	= inclination of satellite orbit plane, radians
Ω	= longitude of the ascending node of satellite orbit, radians
ω	= argument of perigee of satellite orbit, radians
T	= epoch of perigee passage of satellite, seconds
E	= eccentric anomaly of satellite, radians
ρ_o	= observed range from tracker to target, Earth radii
ρ_c	= computed range from tracker to target, Earth radii
$\delta\rho$	= range residual, Earth radii
V_x, V_y, V_z	= satellite velocity components, Earth radii/sec
X, Y, Z	= satellite coordinates, Earth radii
v_i	= observation error in the ith measurement
d	= distance from tracker to geocenter, Earth radii
r	= distance from target satellite to geocenter, Earth radii
m	= set of orbital parameters

Subscripts

T	= target satellite
S	= tracking satellite
*	= nominal trajectory

Introduction

RECENT work in satellite geodesy has demonstrated the feasibility of including the differential equations describing the rotational motion of a deformable earth in an orbit-determination model. By including the Earth dynamical relationships it is possible to process range observations to determine the motion of the pole, the Love numbers h and l, and perhaps to predict the occurrence of major earthquakes. Any parameter which has a direct geometrical effect on satellite range data might be determined in this manner. Therefore it is of interest to consider the determination of geodetic parameters simultaneously with the determination of orbits using range-only data. This paper presents the results of the investigations of techniques for orbit determination using range-only data.

Techniques involving range-only data for orbit determination have been investigated by several researchers in the past. The method of Baker,[1] based on the synthesis of the classical f and g series of celestial mechanics, has been applied to orbit determination using range-only data obtained from ground-based tracking stations. The possibility of using range-only data to determine circular orbits has been also demonstrated by Ball.[2] This technique was dependent on specific geometric properties existing between the tracker and the target satellite's orbit. The feasibility of using two geostationary tracking satellites, called Ephemeris Determination Satellites (EDS), to track target satellites in low-altitude polar and inclined orbits has also been investigated.[3] The accuracies obtained with an orbit-determination computer program using a minimum-variance estimation process and with the use of both range and range-rate measurements from EDS to target satellite were shown to be comparable with those of ground tracking networks.

Space-based tracking stations have the following advantages over ground-based tracking: 1) For a synchronous orbital tracking station the tracking function can be combined with synchronous communication relays. 2) Tracking coverage from space-based stations is increased greatly over that obtainable from an Earth-based station. 3) Because some range measurements can be made outside the atmosphere, the errors that result from atmospheric distortion and refraction are eliminated. 4) Space-based tracking stations can give better geometry between stations and target satellites, therefore providing better accuracy.

Description of the Method

In the following development it has been assumed that both tracking and target satellites are on elliptical orbits. This will not affect the generality of the proposed approach since one can use simple transformations from the expressions developed below to get desired results for the circular or hyperbolic cases.

Received April 10, 1972; revision received September 11, 1972. This work was partially supported under NASA Research Grant NGR 06-002-085. This financial support is gratefully acknowledged.

Index category: Spacecraft Tracking.

* Graduate Student, Mechanical Engineering Department. Member AIAA.

† Associate Professor, Mechanical Engineering, and Associate Director, University Computer Center; presently on sabbatical leave at the University of Newcastle, Department of Electrical Engineering, New South Wales, Australia. Member AIAA.